Supporting Information

Self-Assembly of Supramolecular Triarylamine Nanowires in Mesoporous Silica and Biocompatible Electrodes Thereof

Erol-Dan Licsandru,[a] Susanne Schneider,[b,c] Sophie Tingry,[a] Thomas Ellis,[b] Emilie Moulin,[b] Mounir Maaloum,[b] Jean-Marie Lehn,[c] Mihai Barboiu,[a] and Nicolas Giuseppone*[b]*

[a] E.-D. Licsandru, Dr. S. Tingry, Dr. M. Barboiu
Adaptative Supramolecular Nanosystems Group, Institut Européen des Membranes, ENSCM/UMII/UMR-CNRS 5635, Pl. Eugène Bataillon, CC 047, 34095, Montpellier, Cedex 5 (France)
E-mail: mihail-dumitru.barboiu@univ-montp2.fr

[b] S. Schneider, Dr. T. Ellis, Dr. E. Moulin, Prof. Dr. M. Maaloum, Prof. Dr. N. Giuseppone
SAMS Research Group, University of Strasbourg, Institut Charles Sadron – CNRS, 23 rue du Loess, BP 84047, 67034 Strasbourg Cedex 2 (France)
E-mail: giuseppone@unistra.fr

[c] S. Schneider, Prof. Dr. J.-M. Lehn
ISIS, Institut de Science et d'Ingénierie Supramoléculaires, 8, allée Gaspard Monge 67000 Strasbourg (France)

1. Synthesis

General aspects

All reactions were performed under an atmosphere of argon unless otherwise indicated. All reagents and solvents were purchased at the highest commercial quality and used without further purification unless otherwise noted. Dry solvents were obtained using a double column SolvTech purification system. Yields refer to purified spectroscopically (^{1}H NMR) homogeneous materials. Thin Layer Chromatographies were performed with TLC silica on aluminium foils (Silica Gel/UV_{254}, Aldrich). In most cases, irradiation using a Bioblock *VL-4C* UV-Lamp (6 W, 254 nm and/or 365 nm) as well as Cerium ammonium molybdate stainings were used for visualization. Preparative Adsorption Flash Column Chromatographies were performed using silica gel (silica gel 60 Å, 230 – 400 mesh, 40 – 63 µm, Aldrich). Ultra Performance Liquid Chromatographies coupled to Mass Spectroscopy (UPLC-MS) were carried out on a *Waters Acquity UPLC-SQD* apparatus equipped with a PDA detector (190-500 nm, 80Hz), using a reverse phase column (Waters, BEH C18 1.7 µm, 2.1 mm x 50 mm), and the MassLynx 4.1 – XP software. *^{1}H NMR spectra* were recorded on a *Bruker Avance 400* spectrometer at 400 MHz and ^{13}C spectra at 100 MHz in $CDCl_3$, CD_3OD or DMSO-d_6 at 25°C. The spectra were internally referenced to the residual proton solvent signal ($CDCl_3$: 7.26 ppm, CD_3OD: 3.31 pm, DMSO-d_6: 2.50 ppm for ^{1}H spectrum, and $CDCl_3$: 77.16 ppm, CD_3OD: 49.00 pm, DMSO-d_6: 39.52 ppm for ^{13}C spectrum). For ^{1}H NMR assignments, the chemical shifts are given in ppm. Coupling constants *J* are listed in Hz. The following notation is used for the ^{1}H NMR spectral splitting patterns: singlet (s), doublet (d), triplet (t), multiplet (m), large (l).

Synthetic Pathway

Scheme S1 describes the synthetic pathway for TAA.

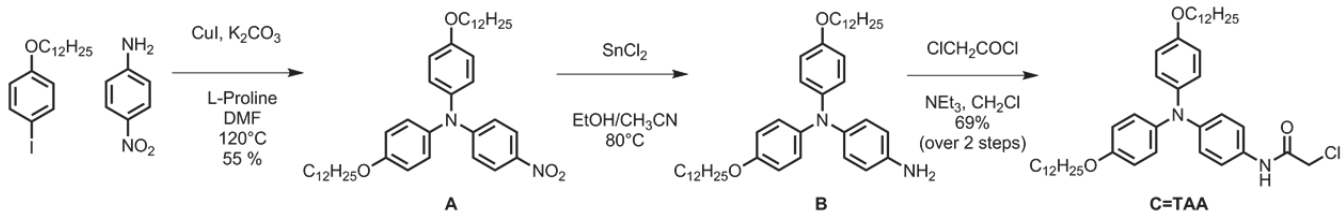

Scheme S1. Synthetic route to access TAA

Synthetic Procedures

Compound A: To one Schlenk flask (large diameter) under argon containing 4-nitroaniline (0.66 g, 4.79 mmol), 1-(dodecyloxy)-4-iodobenzene[1] (6.43 g, 16.57 mmol), copper iodide (0.36 g, 1.92 mmol), potassium carbonate (5.29 g, 38.3 mmol) and L-Proline (0.44 g, 3.83 mmol) was added DMF (20 mL). The reaction mixture was stirred vigorously at 115°C for 7 days. The mixture was cooled down to room temperature and EtOAc (15 mL) was added. The solution was passed through a pad of celite and washed with EtOAc (300 mL) to remove all copper salts. The resulting organic phase was concentrated under reduced pressure. Further purification of the crude mixture by column chromatography (SiO_2, Pentane → Pentane/Et_2O: 98/2) afforded triarylated compound **A** in 55% yield (1.72 g).

^{1}H NMR ($CDCl_3$, 400 MHz, 25°C) δ = 7.99 (d, ^3J = 9.4Hz, 2H), 7.11 (d, ^3J = 9.0Hz, 4H), 6.89 (d, ^3J = 9.0Hz, 4H), 6.75 (d, ^3J = 9.4Hz, 2H), 3.95 (t, ^3J = 6.6Hz, 4H), 1.82 – 1.75 (m, 4H), 1.50 – 1.43 (m, 4H), 1.37 – 1.23 (m, 32H), 0.88 (t, ^3J = 6.9Hz, 6H); ^{13}C NMR ($CDCl_3$, 100 MHz, 25°C) δ = 157.3, 154.2, 138.9, 138.0, 128.1, 125.6, 115.7, 115.6, 68.3, 31.8, 29.6 (4x), 29.3, 29.2 (2x), 26.0, 22.6, 14.1; ESI-MS: m/z calculated for $C_{42}H_{63}N_2O_4$ $[M+H]^+$ 659.48; found 659.49.

Compound B: A solution of compound **A** (1.52 g, 2.78 mmol) and tin(II) chloride dihydrate (7.52 g, 33.34 mmol) in acetonitrile (45 mL) and ethanol (45 mL) was stirred overnight under reflux. After that time, the solution was cooled down to room temperature and diluted with ethyl acetate (300 mL). The organic phase was washed with Na_2CO_3 sat. (2 x 200 mL) and brine (100 mL), dried over Na_2SO_4 and concentrated under reduced pressure. The resulting product was clean enough to be used as such in the next step.

^{1}H NMR (MeOD, 400 MHz, 25°C) δ = 7.47 (d, ^3J = 9.0Hz, 4H), 7.37 (d, ^3J = 8.8Hz, 2H), 7.15 (d, ^3J = 9.0Hz, 4H), 6.66 (d, ^3J= 8.8Hz, 2H), 4.09 (t, ^3J = 6.5Hz, 4H), 3.32 – 3.02 (brs, 2H), 2.09 – 2.02 (m, 4H), 1.82 – 1.75 (m, 4H), 1.71 – 1.66 (m, 32H), 1.32 (t, ^3J = 6.9Hz, 6H); ^{13}C NMR (MeOD, 100 MHz, 25°C) δ = 157.5, 154.4, 139.1, 138.2, 128.2, 125.7, 115.9, 115.9, 68.5, 32.1, 29.8, 29.8, 29.8, 29.7, 29.6, 29.5, 29.4, 26.2, 22.8, 14.3; ESI-MS: m/z calculated for $C_{42}H_{65}N_2O_2$ $[M+H]^+$ 629.50; found 629.64.

Compound C: A solution of compound **B** (0.41 g, 0.66 mmol) and triethylamine (110 µL, 0.80 mmol) in dichloromethane (9 mL) was added dropwise to a cooled solution of chloroacetylchloride (63 µL, 0.79 mmol) in dichloromethane (10 mL) at 0°C. The reaction mixture was heated slowly to room temperature for 12 h. It was then diluted with diethyl ether (60 mL) and the organic phase was washed with NH_4Cl sat. (2 x 60 mL) and brine (60 mL), dried over Na_2SO_4 and concentrated under reduced pressure. Further purification of the crude mixture by column chromatography (SiO_2, Cyclohexane →

[1] S. Rondeau-Gagné, C. Curutchet, F. Grenier, G. D. Scholes, J.-F. Morin, *Tetrahedron* 2010, **66**, 4230–4242.

Cyclohexane/EtOAc: 3/1) afforded triarylated compound **C** in 69% yield over 2 steps (0.32 g). ^{1}H NMR (DMSO-d$_6$, 400 MHz, 25°C) δ = 10.14 (s, 1H), 7.40 (d, ^{3}J = 9.0Hz, 2H), 6.91 (d, ^{3}J = 8.9Hz, 4H), 6.84 (d, ^{3}J = 8.9Hz, 4H), 6.79 (d, ^{3}J= 9.0Hz, 2H), 4.19 (s, 2H), 3.90 (t, ^{3}J = 6.6Hz, 4H), 1.71 – 1.64 (m, 4H), 1.40 – 1.35 (m, 4H), 1.32 – 1.19 (m, 32H), 0.85 (t, ^{3}J = 6.9Hz, 6H); ^{13}C NMR (DMSO-d$_6$, 100 MHz, 25°C) δ = 164.0, 154.7, 144.4, 140.42, 131.8, 125.6, 121.1, 120.6, 115.3, 67.6, 43.5, 31.2, 29.0, 29.0, 28.9, 28.9, 28.7, 28.7, 25.5, 22.0, 13.9; ESI-MS: m/z calculated for $C_{44}H_{65}ClN_2O_3$ $[M]^+$ 704.47; found 704.76.

2. XPS Measurements

X-ray photoelectron spectrometry (XPS) analyses were performed on a KRATOS Axis Nova (Kratos Analytical, Manchester, United Kingdom), using AlKα radiation, with 20 mA current and 15 kV voltage (300 W), under a base pressure of 10^{-8} to 10^{-9} Torr in the sample chamber. The incident monochromatic X-ray beam was focused on a 0.7 mm x 0.3 mm area of the samples bearing surface. XPS survey spectra were collected in the range of -10 to 1200 eV, with a resolution of 1 eV, at a pass energy of 160 eV. The high resolution spectra for all the elements identified in the survey spectra were collected using a pass energy of 20 eV and a step size of 0.1 eV. XPS data fitting were performed making use of the Vision Processing software (Vision2 software, Version 2.2.10), and mixed Gaussian-Lorentzian curves. The linear background was subtracted before correction of the peak areas. The binding energy of the C 1s peak was normalized to 285 eV. Elemental analyses were performed using a scanning electron microscope (Quanta 200-FEI) equipped with an energy-dispersive X-ray spectroscopy system (EDX). Elemental nitrogen analysis was performed on a Perkin Elmer 2410 Series II CHNS/O ANALYZER 2400.

Table S1. XPS results of different electrode modifications

Sample	Element (%)	C	O	Si	N	S
Porous Bare	Atomic conc.	43.28	34.69	15.68	4.25	1.5
	Mass conc.	31.62	33.76	26.79	3.62	2.92
C6 Modified	Atomic conc.	53.6	25.75	20.65	0.0	0.0
	Mass conc.	39.35	25.18	35.47	0.0	0.0
TAA Doped	Atomic conc.	48.59	30.8	17.58	2.15	0.0
	Mass conc.	32.89	27.78	27.82	1.7	0.0

Calculation of the number of pores filled with TAA

To determine the area of the electrode occupied by TAA, we assume that all the nitrogen signal arises from the triarylamine. Using the dimensions of two triarylamine molecules (Figure 1), we determine an area of: 1.5 nm x 2.3 nm = 3.45 x 10^{-18} m^2

Area per nitrogen (4 nitrogens per cell) = 3.45 x 10^{-18} m^2 / 4 = 8.63 x 10^{-19} m^2

Area of a single nitrogen atom = π x (155 pm)^2 = 7.54 x 10^{-20} m^2 (assuming that the area of the nitrogen atom corresponds to the covalent radius of a circle)

Ratio of TAA area to nitrogen = 8.63 x 10^{-19}/ 7.54 x 10^{-20} = 11.5

Percent of molar nitrogen by XPS = 2.15%

Percent of triarylamine = 2.15 % x 11.5 = 24.6 %

Regarding the initial approximation, and the fact that pores occupy 66 % of the total surface (see next section), we can conclude that about 1/3 of the pores are filled with triarylamines, which is in a good agreement with AFM observations.

3. Porous Electrode Area

By comparing the CVs of $Ru(NH_3)_6^{3+}$ at the gold electrode and at the porous electrode, it is possible from the i_p (peak current density) values to evaluate the electroactive surface area using Randles–Sevcik equation (Eq. 1):

$$i_p = 0.4463\, nFAC \left(\frac{nFvD}{RT}\right)^{\frac{1}{2}}$$

With i_p : current maximum (A), n : number of electrons transferred in the redox event (1), A : electrode area (cm^2), F : Faraday constant (C mol^{-1}), D : diffusion coefficient of $Ru(NH_3)_6^{3+}$ (cm^2/s), C : concentration (mol/L), v : scan rate in V/s, R : gas constant, T : temperature (°C)

For identical experimental conditions, and by considering that the diffusion coefficient of $Ru(NH_3)_6^{3+}$ in an aqueous solution of $NaNO_3$ is similar at the gold electrode surface and within the pores of the porous electrodes, it results that: $i_{p\ gold\ electrode}/i_{p\ porous\ electrode} = A_{gold}/A_{porous\ electrode}$.

$A_{porous\ electrode} = A_{gold} * i_{p\ gold\ electrode}/i_{p\ porous\ electrode}$

Considering that the gold surface area is 0.226 cm^2, the area of the porous electrode is estimated to 0.15 cm^2. Thus, around 66% of the surface area is accessible when the electrode is covered by the porous layer.

4. Contact Angle Measurements

Measurements were performed on a GBX Digidrop apparatus by depositing 12±1 µL pure-water droplets on the electrode surface.

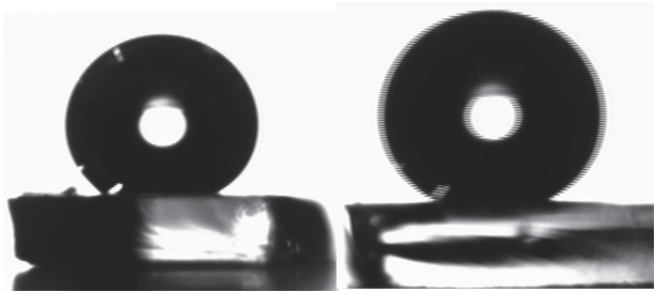

Figure S1. Contact angle measurements of the C6-modified surface (141.5°, left) and the TAA-modified surface (149.3°, right).

5. Cyclic Voltammetry

Electrochemical measurements were performed on a potentiostat (Ametek, Versa Stat 3) at room temperature in a 0.1 M aqueous solution of $NaNO_3$, with a conventional three-electrode system composed of a stainless steel auxiliary electrode, an Ag/AgCl reference electrode, and a mesoporous silica ITO films of 20 mm^2 as working electrode. Cyclic voltammograms (CV) were measured in the presence of 5 mM $Ru(NH_3)_6^{3+}$ (ruthenium hexamine chloride) in 0.1 M aqueous solution of $NaNO_3$ at scan rate of 20 $mV.s^{-1}$. Linear scan voltammetry measurements were determined in dioxygen-saturated phosphate buffer at pH 5 after stabilization of the biocathode open circuit potential at scan rate 3.3 $mV.s^{-1}$. The current density was determined from the geometrical surface area of the electrodes.

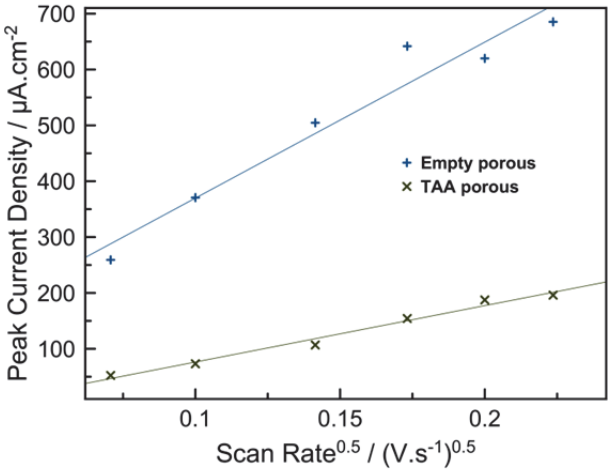

Figure S2. Linear peak current density (i_{peak}) as a function of the square root of the scan rate ($v^{1/2}$) for the doped triarylamine mesoporous electrode and the porous electrode with "empty" pores in the same redox probe conditions, supporting that electron-transfer process is only limited by the diffusion of the redox species.

Control Experiments

We studied the electrochemical response of the species Ru^{3+} in the presence of tridodecylamine introduced into the pores. No increase of the current response was observed for pores loaded with tridodecylamine compared with the C6-functionalized electrode (Figure S3). This experiment confirm that a simple amine molecule is not able to promote the transfer of electrons.

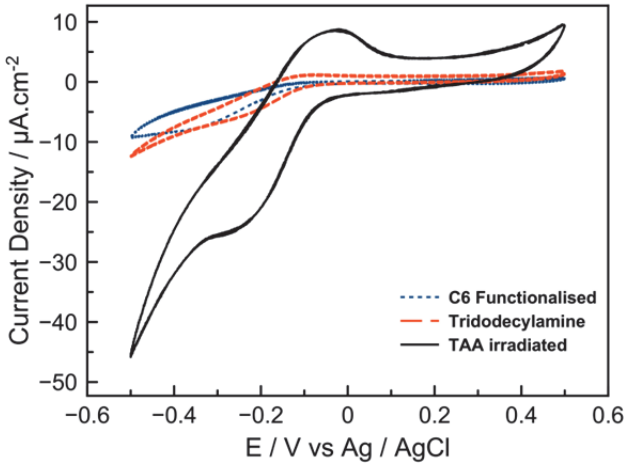

Figure S3. Cyclic voltammograms for the Ru^{3+} redox probe (5 mM) using different electrodes: after C6 functionalization (blue doted line), after doping with TAA irradiated (black line), and after doping with tridodecylamine (orange dashed line), (0.1 M $NaNO_3$, $\nu = 20$ mV.s^{-1}).

The stability of the electrodes doped by TAA nanowires was regularly checked over a period of one month by repeating cyclic voltammetry of the electrodes in solutions containing the redox probe $Ru(NH_3)_6^{3+}$. The intensity and the position of the oxidation and reduction peaks was nearly the same pointing out the stability of the overall structure.

6. Electrochemical impedance spectroscopy

In order to determine the charge transfer properties of the modified silica layers, Electrochemical Impedance Spectroscopy (EIS) was performed in 0.1 M phosphate buffer (pH 7) containing the redox probe potassium hexacyanoferrate trihydrate $Fe(CN)_6^{3-}$/ $Fe(CN)_6^{4-}$ (10 mM). The frequency range on EIS was varied from 10 kHz to 0.1 Hz, with 10 points per decade, at the half wave potential ($E_{1/2}$ = 0.208 V).

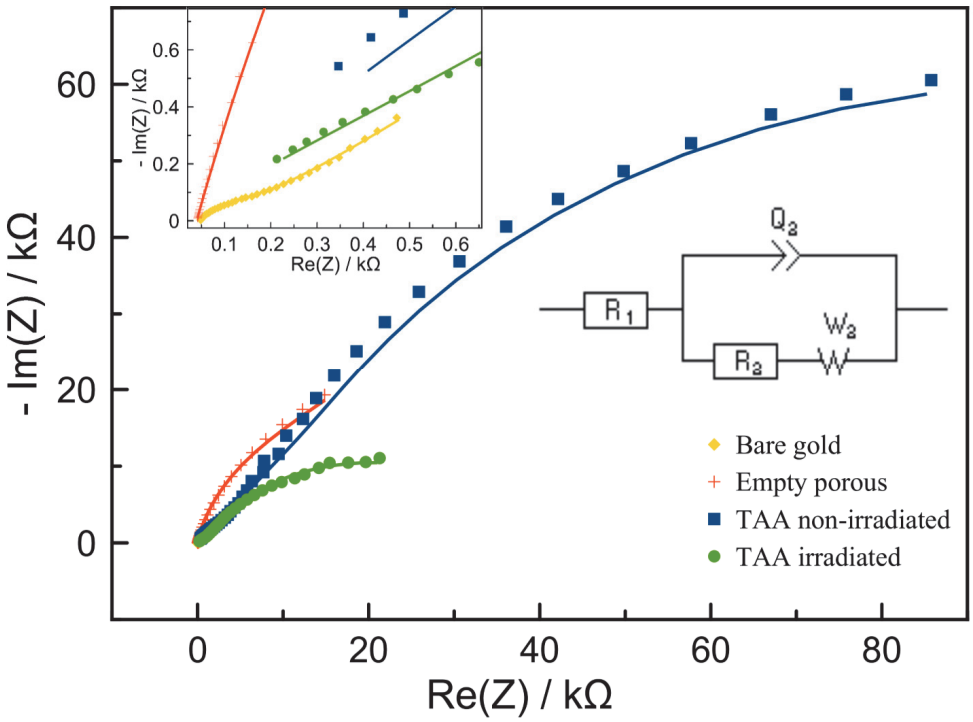

Figure S4. Nyquist plot of the impedance response for each tested electrode (experimental data as marks and fits with Randels circuit model as lines). Inset shows the higher frequency response (marks) and the corresponding fits with Randles circuit model (lines).

A Randles circuit[2] was modelled as described in the inset of Figure S4, where R_s is the resistance of the electrodes/solution, R_{ct} is the resistance from the charge transfer, Q is the constant phase element coefficient, R_{dif} is the diffusion resistance, and T_d Nernst diffusion layer thickness.

Table S2. Modeled parameters for the Randles circuit.

Electrode	R_s (Ω)	Q	A	R_{ct} (Ω)	R_{dif} (Ω)	T_d	Area
Bare Gold	46	7.3E-05	0.730	165.7	1904	2.2	0.255
Empty Porous	39	5.0E-06	0.894	26733	41037	0.76	0.35
TAA non-irradiated	0	1.8E-06	0.603	10385	204223	0.10	0.331
TAA irradiated	0	1.0E-05	0.480	156.8	48182	0.07	0.336

The Randles circuit model fits the data quite well despite the 100 nm silica layer. From the model, the charge transfer resistance should provide a good approximation of the resistance from the wire. The bare gold charge transfer resistance can be used as the charge transfer resistance intrinsic to the gold layer and the transfer to the redox probe.

[2] J. E. B. Randles, *Discuss. Faraday Soc.* 1947, **1**, 11–19.

Assuming that the silica layer thickness determined by SEM corresponds to the thickness of the path length of the TAA (91.3 nm), and that the determined polarization resistance arises primarily from TAA charge transfer, the charge transfer resistivity of each layer can be determined by:

$$\rho = \frac{RA}{l}$$

Table S3. Charge transfer resistivity of modeled Randles circuit was chosen to fit the impedance data.

Electrode	**Rct / Ω**	**Area / cm^2**	**Resistivity/ Ω.m**
Bare Gold	165.7	0.255	4.63E+04
Empty Porous	26733	0.35	1.03E+07
TAA non-irradiated	10385	0.331	3.77E+06
TAA irradiated	156.8	0.336	5.77E+04

7. Control experiments with bare gold biocathodes

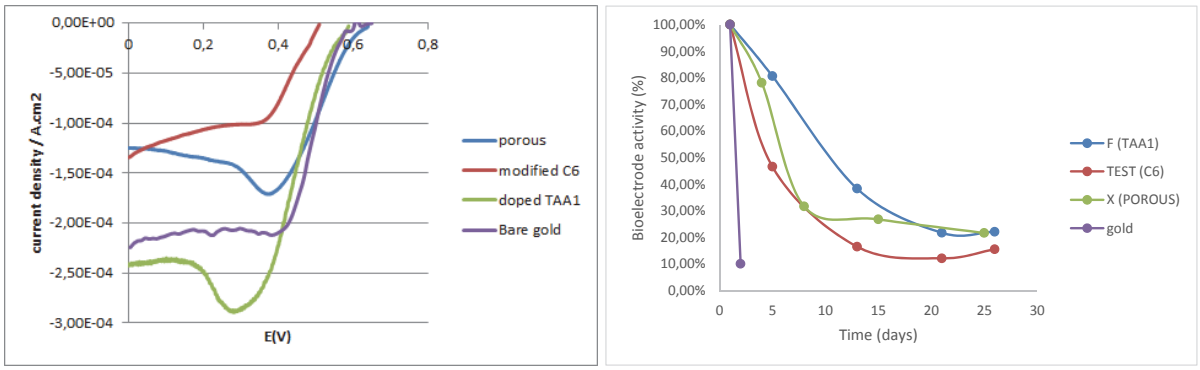

Figure S5. (left) Bare gold electrode with immobilized enzymes in nafion exhibits similar performance to that of the doped mesoporous electrode. However, the enzyme layer does not stick properly and usually collapse on the gold surface and thus the stability of the resulting electrode is restricted to only one day (right). In the case of the hybrid electrode, the porous silica layer ensures the confinement of triarylamine units within the pores and improves the stability of the enzyme layer at the electrode surface at least over 10 days.

8. ^{1}H and ^{13}C NMR of TAA

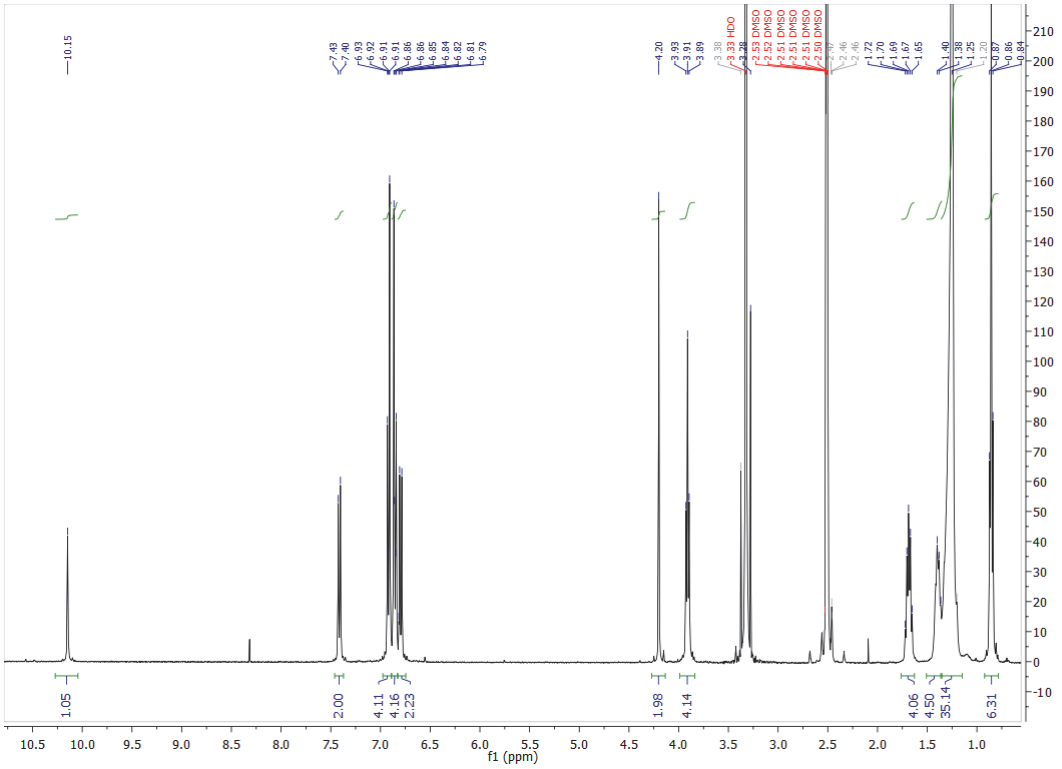

Figure S6. ^{1}H-NMR of Compound **TAA** in DMSO-d_6

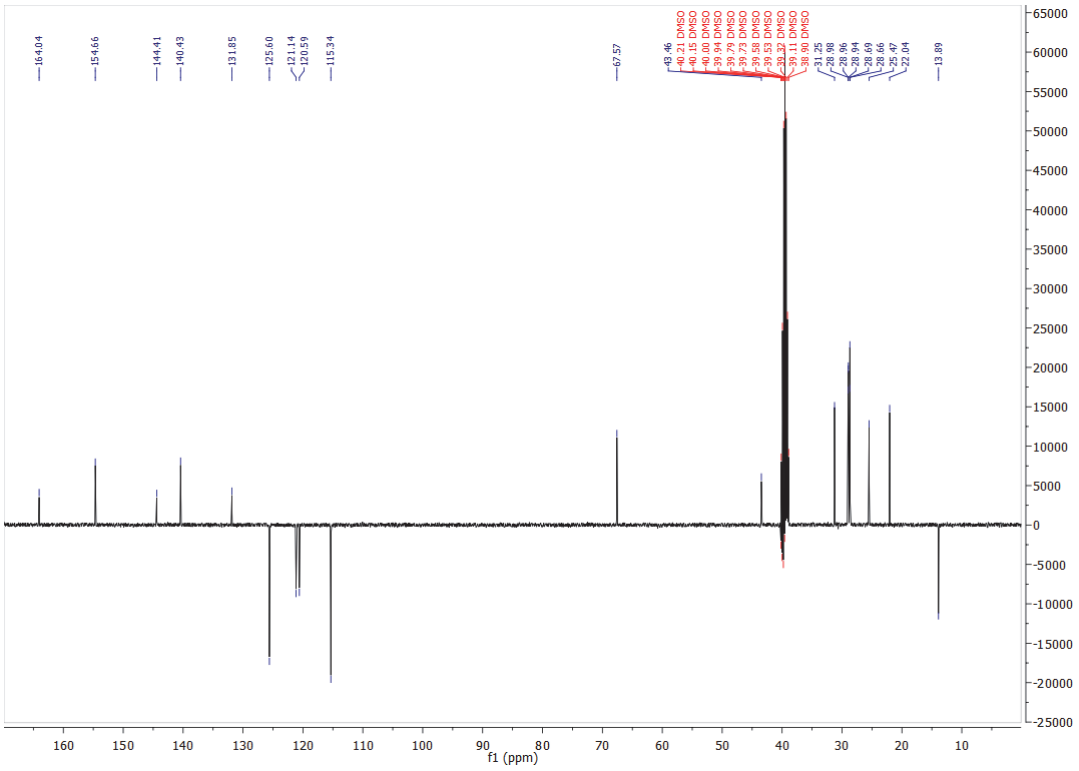

Figure S7. ^{13}C-NMR of Compound **TAA** in DMSO-d_6.